Flow Simulation of a Mixing Vessel Incorporating Blade Element Theory

D.A. Niclasen, M. Rudman, H.M. Blackburn and J. Wu
CSIRO Building, Construction and Engineering (BCE), Highett Victoria

ABSTRACT

Computer simulations of flow within an impeller-stirred mixing tank have been carried out, and the results compared with those obtained experimentally. Blade element theory and experimental results are used in order to allow the exclusion of the impeller from the computation region. It is shown that the solution obtained is sensitive to the boundary conditions applied. Although the solution was qualitatively correct, a close match to experimental data was not achieved.

Nomenclature

I	Turbulence intensity $u'/\overline{u}$
k	Turbulent kinetic energy
l	Integral length scale
$\overline{u}$	Mean velocity (component)
u'	Fluctuating velocity component
Uz	Axial velocity component
ϵ	Dissipation

1. INTRODUCTION

Impeller-stirred mixing vessels are widely used within the minerals processing industry, and it is desirable to be able to perform accurate simulations in the design phase in order to ensure various flow criteria can be met in practice. These may include minimum shear stresses near the tank walls in order to prevent the build up of scale, or may require that multiple phases be mixed within a certain time. Often the fluid within the tank is non-Newtonian, and the flow is usually turbulent.

Alteration of the flow field within a tank can be achieved by changing the speed of rotation of the impeller, changing the type of impeller, or changing the geometry of the tank. Geometry changes may include the use of more than one impeller, the use of different impellers, changing the location of the impeller in the tank, and redesign of tank baffles. Experimental investigation of design variables can be costly and time consuming both in terms of physical alterations and data collection. The use of computational methods to predict the tank flow is very attractive due to its relatively low cost and the ease with which changes to the system being modelled can be implemented and investigated.

This paper presents results of a computational study of an impeller-stirred mixing vessels using the commercial CFD code "CFX–4.1". This is a multi-block finite volume code which is well suited to the moderate geometrical complexity of the current problem. Rather than meshing and solving the region around the impeller, which normally requires an extremely large number of mesh points, the impeller region is excluded from the computational domain and the boundary conditions are set using a combination of experimental observations and a separate blade element code.

The case presented here is for a cylindrical tank fitted with an A310 impeller, which has aerofoil shaped blades. Geometric details of the tank are presented in figure 1. The impeller shaft extends beyond the impeller to the base of the tank. This particular case has been studied experimentally at CSIRO BCE,

allowing detailed comparisons to be made between computer simulations and experimental measurements of the flow field.

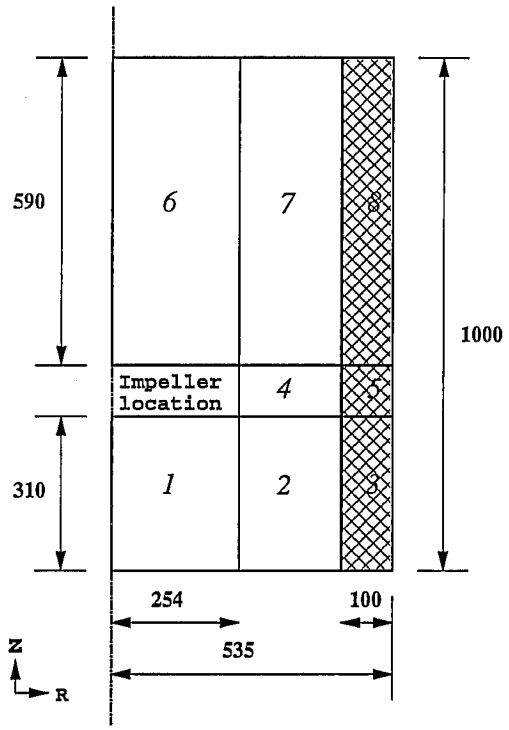

Figure 1: Tank geometry, including block numbers for the multi-block grid used. Shaded region represents the baffles. The impeller sits at the mid-height of the impeller region.

2. EXPERIMENTAL DETAILS

A TSI 2D fibre laser-doppler velocimetry (LDV) system was used for velocity measurements. A Karel S-10 robotics system was used to traverse the fibre probe. The probe could be positioned with an accuracy of 0.5 mm. The LDV system and the robot were interfaced to a computer so that the LDV operation and probe positioning were automatically controlled. The uncertainty of an instantaneous velocity measurement was approximately 0.3% in the present application. Velocity distributions in the mixing tank were obtained by traversing the LDV probe through the tank automatically. Time-mean velocity data at each position was obtained using a sampling time of 90 sec at a typical data rate of 60 pts/sec. The velocity bias inherent in LDV was corrected using transit time weighting to reduce the error in the mean values. An example of the measured velocity profile immediately below the impeller can be seen in figure 2.

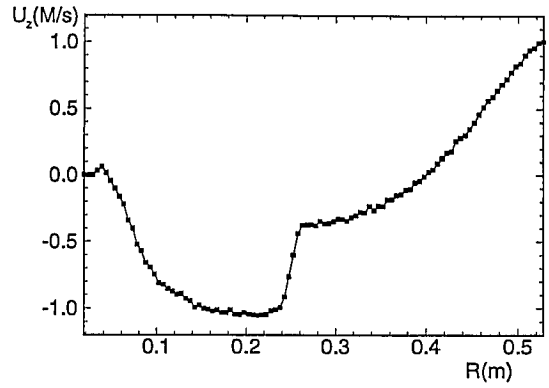

Figure 2: Measurements of the axial velocity component obtained immediately below a 460 mm diameter A310 impeller.

3. NUMERICAL MODELLING

3.1 Model Details

In order to substantially reduce the number of mesh points required, flow around the impeller zone was set on the basis of experimentally measured velocity profiles coupled with blade element theory.

Experiments carried out at CSIRO BCE on impeller-stirred mixing tanks have shown that the velocity profile immediately below an impeller is a function primarily of the impeller geometry, and is not greatly influenced by the overall flow within the tank. This knowledge can be used to set the axial component of the velocity below the impeller region. As shown in figure 2 the axial profile can be suitably modelled using a linear piecewise approach, with four line segments used in this study.

In order to calculate the component of velocity in the azimuthal direction, blade element theory is used (Wallis 1983). Using the angle of attack and the physical character-

istics of the impeller blades, the azimuthal velocity is calculated from the axial velocity and the lift produced by the blades. The theory had previously been incorporated into a computer code at CSIRO BCE as part of an industry-funded project. That code has been adapted here in order for it to be called by CFX–4.1 to set the boundary conditions around the impeller region.

Typical mesh sizes employed for the problems discussed in this paper had $35 \times 45 \times 30$ mesh points, which is a substantial reduction on the number of points required if the impeller is included in the mesh. Figure 3 shows the layout of a typical computational mesh, although the total number of points shown has been reduced to improve clarity. Various convection schemes and turbulence models were tested, as discussed in further sections of this paper. All solutions were for steady state flow. A simulation with twice the number of mesh points in each coordinate directions was performed to test for grid–dependency using the second-order quadratic upwind scheme for convection, and the results were found to be substantially the same as for the coarser mesh. Figure 4 shows the comparison between the two meshes for the axial velocity profile immediately beneath the impeller region.

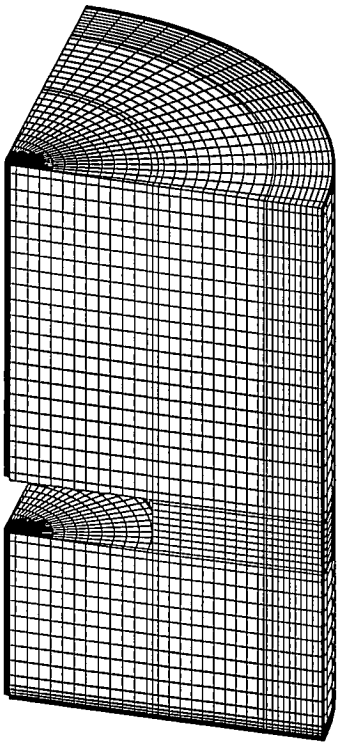

Figure 3: Typical mesh layout.

3.2 Convection Schemes

Initially the problem was solved using the default options in CFX-4.1, namely the hybrid scheme for the advection term, and the k-ϵ turbulence model. The hybrid scheme is primarily an upwinding scheme with some modifications. When the mesh Peclet number is less than 2, second-order convection is used instead of the upwind scheme. The scheme is only first-order accurate.

Physical measurements showed that the flow separated from the side wall of the tank midway between the baffles at a height of 0.73 mm, with a recirculation zone occurring above this height. Figure 5 shows the maximum near-wall velocity along the side wall of the tank for the simulation using the hybrid scheme, compared to the experimental results. The flow separation occurs where the velocity changes sign. The initial simulation using the first-order accurate scheme failed to predict the flow separation, apart from near the top of the tank where a very small recirculation zone was observed. This feature can be observed in the vector plot of figure 6. It was thought that the numerical diffusion introduced by the first-order upwind scheme was responsible for the lack of separation. This was consistent with a laminar flow solution where the relatively high numerical diffusion prevented flow separation. In order to test this hypothesis higher order convection schemes were tested.

Subsequent simulations were all performed using higher order convection schemes for the momentum equation and the hybrid scheme for other equations. The main scheme tested was the quadratic upwind scheme (QUICK) provided by CFX. This scheme is third-order accurate for the advection term, however the code still uses a second-order central difference scheme for all other terms. The use of a higher order scheme resulted in the solution separating from the side wall of the tank

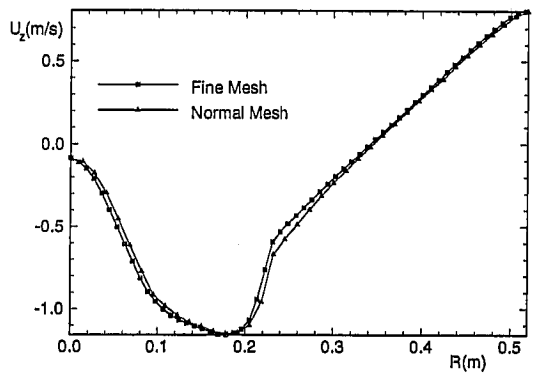

Figure 4: Comparison of axial velocity profile below impeller for different mesh resolutions.

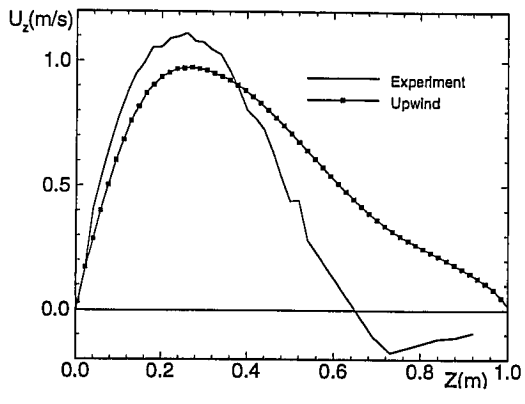

Figure 5: Comparison of axial wall velocity profiles for first order upwind convection and experimental results.

at heights ranging from 0.73 m to 0.93 m, depending upon the boundary conditions used under the impeller region. This will be discussed further in the next section of this paper. A typical flow pattern on a slice midway between the baffles can be seen in figure 7.

3.3 Boundary Conditions

The default turbulence model used in CFX is the k-ϵ model, a two-equation closure whereby equations for the turbulent kinetic energy and turbulence dissipation are solved. This model has the advantage of being relatively cheap to use in terms of computation cost, and has been applied widely in turbulence modelling. The k-ϵ model was used for all of the simulations reported in this paper.

One of the requirements when using turbulence models is to determine the appropriate boundary conditions for turbulence quantities. In the case of the k-ϵ model used for the present work, it is necessary to set the values of both k and ϵ at any inflow boundaries.

The value for k used at the inflow boundary was derived from the experimental data using the relationship

$$k = \frac{3}{2} I^2 \overline{u}^2. \qquad (1)$$

Experimentally it was found that the average value of the turbulence intensity I was around 30%, so this value was used to derive k, along with mean axial velocity over the impeller outlet. The value of ϵ is then derived from

$$\epsilon = \frac{k^{3/2}}{l} \qquad (2)$$

where l is an appropriate length scale, taken to be slightly less than half the impeller diameter in this case. Tests showed the solution to be relatively insensitive to the boundary conditions for ϵ.

Using a value of k of 0.022 which was derived from a turbulence intensity of 30%, it was found that the flow separation from the side wall of the tank occurred at a height of 0.84 m from the base of the tank, whereas experimentally it was found to occur at a height of 0.73 m. In order to determine the effect of the boundary condition for turbulent kinetic energy, the simulation was performed with several different values of k, as indicated in figure 8, where the vertical component of velocity near the tank wall is shown. From this it is evident that the choice of the turbulent kinetic energy at the impeller boundary plays an important role in obtaining an accurate simulation. The use of higher values of k leads to a higher value of turbulent viscosity, increasing the amount of diffusion.

The experimental data were examined for distribution of turbulent kinetic energy was

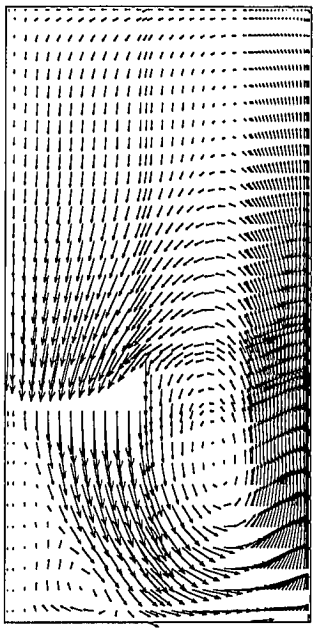

Figure 6: Vector plot on a vertical slice midway between baffles. Solution used first order upwind convection.

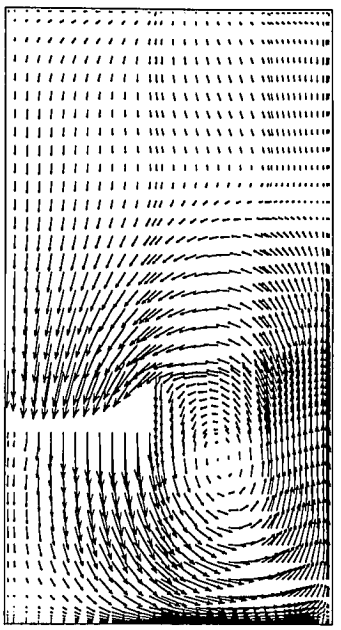

Figure 7: Vector-vector plot on a plane between the baffles using quadratic upwind convection. The flow separation from the side wall is clearly visible.

underneath the impeller. Figure 9 shows that the level of the turbulent kinetic energy varies greatly, with two distinct peaks. These peaks correspond to the location of the hub and blade tip of the impeller. Since the flow solution is highly dependent on the setting of the turbulent kinetic energy, the code which sets the boundary conditions for the axial and swirl velocity under the impeller was modified so that a variable profile could be set for both the turbulent kinetic energy and the dissipation. This was done using a piecewise–linear approach, with the number of linear segments able to be varied to suit the required profile; five segments were used to model the profile in figure 9.

The results for this method showed no significant improvement on those obtained using a constant value of kinetic energy on the boundary, as seen by the result labelled "variable k-profile (iso)" in figure 10.

No experimental data were available concerning turbulence intensity in directions other than axial, so the previous result assumed isotropic turbulence under the impeller. This was felt to be a poor assumption as the flow is observed to be anisotropic in this region. In the absence of experimental data, it was next assumed that the level of turbulence intensity in the radial direction would be negligible owing to the low velocities in this direction. In the azimuthal direction, the velocities are approximately 30% of those in the axial direction, so the turbulence intensity was assumed to be about 30% of the axial value. These assumptions change equation (1) to

$$k = \frac{1.3}{2} I^2 \overline{u_z}^2. \tag{3}$$

The results using this value are also shown in figure 10, with the line labelled "variable k-profile (noniso)". Once again there was little improvement over the previous result.

4. DISCUSSION

The results presented have demonstrated that the solution obtained using a turbulence model such as the k-ϵ model can be influenced strongly by the boundary conditions needed

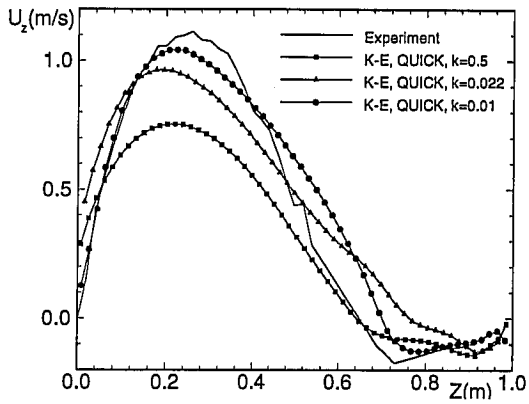

Figure 8: Comparison of axial wall velocity profiles for different boundary values of turbulent kinetic energy k (uniform on radius).

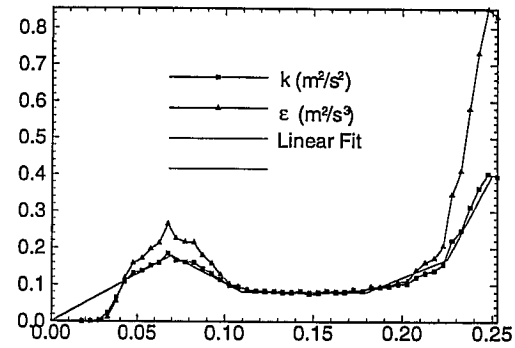

Figure 9: Profile of turbulent kinetic energy under impeller obtained using equation (1). Values of ϵ have been modelled using equation (2).

by the model. Although in some cases these values may be known in advance, this is generally not the case. In order to obtain suitable values, experiments are required. The use of "typical" values could be a dubious practice as the solution can be sensitive to the boundary values chosen.

The flow in an impeller-stirred mixing vessel is difficult to model accurately using simple turbulence models. This is due primarily to the nature of the flow, as it is a highly swirling flow with flow separation from the walls, both flow features which models such as k-ϵ are poor at reproducing correctly (Wilcox 1993). The next stage of this work will investigate the use of Reynolds stress models to investigate if they are able to more accurately reproduce the experimental results.

At this stage there is still insufficient experimental data available for some of the features of the computational solution to be verified. In particular, the computational solution shows that the flow at the top of the tank swirls in the opposite direction to the rotation of the impeller over a substantial area of the surface. This can be seen in figure 11, where the velocity vectors close to the surface have been plotted. The impeller is rotating in the anticlockwise direction, shown by the velocity vectors close to the impeller shaft, however the flow along most of the outer wall of the tank is swirling in a clockwise direction.

This feature of the flow was observed for all computational solutions, irrespective of the boundary conditions for the kinetic energy, and is produced by the impingement of flow from the impeller on to the tank baffles. Flow in the opposite direction to the rotation of the impeller was observed in the experimental rig, however time–averaged statistics are not yet available for comparison. The flow was observed to move in the opposite direction in surges, making it difficult to judge the direction of the mean flow visually. It is planned that experimental data in this region will be collected in the future in order to compare with the computed flow field.

5. CONCLUSIONS

The simulations presented here are in reasonable qualitative and quantitative agreement with the flows observed experimentally, including prediction of separation zones. Simulation results were shown to be sensitive to boundary conditions supplied for turbulence quantities, but use of experimentally derived values did not succeed in delivering an ideal match between experimental and simulated flows. This suggests that the turbulence model requires refinement.

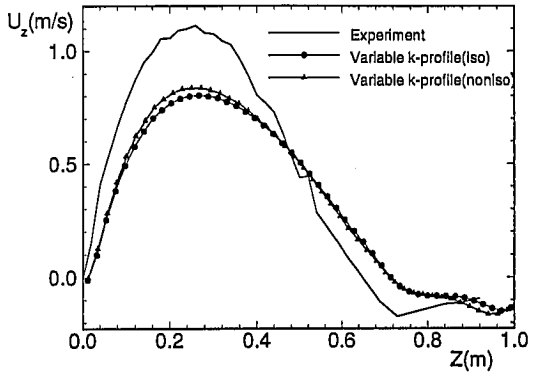

Figure 10: Comparison of axial wall velocity profiles using experimentally derived profile for kinetic energy on lower impeller region boundary.

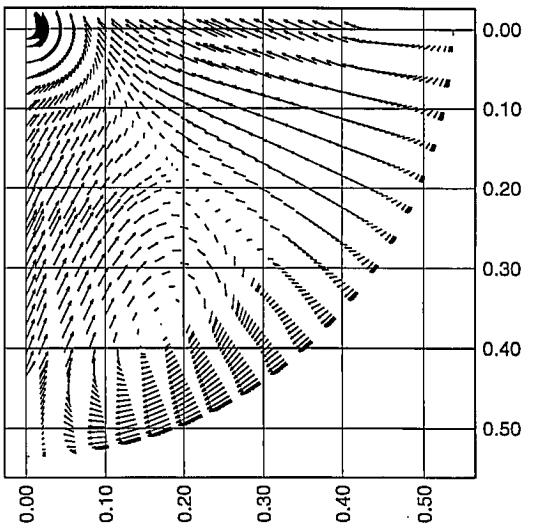

Figure 11: Velocity vectors near top of tank showing flow swirling in the opposite direction to the rotation of the impeller.

Overall, the results indicate the potential utility of simplified models for representation of impeller flows in modelling of mixing vessel flows.

ACKNOWLEDGEMENTS

The authors wish to acknowledge the support from the sponsors of AMIRA project P419.

References

Wallis, R. A. (1983). *Axial Flow Fans and Ducts*, Wiley-Interscience.

Wilcox, D. C. (1993). *Turbulence Modeling for CFD*, DCW Industries.